Pure & Appl. Chem., Vol. 59, No. 11, pp. 1465–1476, 1987.
Printed in Great Britain.

Site-directed processing of N-linked oligosaccharides: the role of three-dimensional structure

Jeremy P. Carver and Dale A. Cumming

Department of Medical Genetics, University of Toronto, Canada M5S 1A8

Abstract - The discovery of extensive conformational averaging in some oligosaccharides of biological interest has necessitated a revision of our previous methodology for the quantitative interpretation of the nuclear Overhauser effect (NOE) in ^{1}H NMR measurements. The calculation of ensemble averaged NOE's requires the determination of statistical weights from some potential energy function. As a result, comparison of calculated and observed NOE's provides a method for the evaluation of different potential energy functions. The utility of this approach is illustrated by calculations for the Manα1,3 linkage in a biantennary complex class glycopeptide. The resulting detailed knowledge of the three-dimensional structures of intermediates in the oligosaccharide biosynthetic pathway has yielded insights into the regulation of this process. In particular, a possible mechanism for the differential processing of N-linked oligosaccharides at different glycosylation sites of the same glycoprotein has been proposed. Unlike previous suggestions, based on differential accessibility, this model allows for processing at different sites to proceed along different branches of the biosynthetic pathway. The essence of the model is that interactions between the oligosaccaride and the protein at the glycosylation site can stabilize three-dimensional structures which are no longer substrates for one of the subsequent processing enzymes in the pathway thereby steering the biosynthesis. We term this model 'Site-directed Processing'.

INTRODUCTION

Almost a decade ago Jean Montreuil predicted that the biantennary N-linked oligosaccharides from the glycoproteins of higher organisms would have well defined three-dimensional structures with the major site of flexibility being the Manα1,6 linkage in the core (ref. 1). In the last five years ^{1}H NMR has provided the detailed evidence with which the validity of Montreuil's speculations can be evaluated (refs. 2-14). The NMR results suggest that the torsional angles about glycosidic linkages are restricted to narrow ranges of values. However, as Lemieux and Bock (ref. 13) have pointed out, this restriction can be accounted for by van der Waals interactions and the exo-anomeric effect, thus leaving the role of the intramolecular hydrogen bonds, originally suggested by Montreuil, as a matter of controversy. In this report we will demonstrate how quantitative NOE measurements can begin to address this issue and then go on to illustrate how the resulting detailed knowledge of the three-dimensional structures of the N-linked oligosaccharides has yielded insights into the mechanisms for the regulation of processing in their biosynthetic pathway.

NMR DETERMINATION OF THE THREE-DIMENSIONAL STRUCTURES OF N-LINKED OLIGOSACCHARIDES

Nuclear Overhauser effect

In recent studies (refs. 2-9) we have used ^{1}H NMR methods to explore the three-dimensional structures of a wide variety of N-linked oligosaccharides. The methods that we have used to deduce these structures differ from those used conventionally and it is therefore worthwhile to review the reasons for these differences.

NMR effects can be loosely categorized into those that are transmitted through bonds (scalar effects such as coupling constants) and those that are transmitted through space (dipolar effects such as the nuclear Overhauser effect or 'NOE'). Effects transmitted through space provide an opportunity for the determination of internuclear distances, provided that the distance dependance of the effect is well understood, as is the case for NOE's (see ref. 15). The NOE experiment is performed by pre-irradiating the resonance of one hydrogen (usually a well isolated resonance) and detecting the changes in intensity which occur for

the signals of other hydrogens close in space to the saturated hydrogen. For oligosaccharides and glycopeptides the effects are small, generally consisting of perturbations in the intensity of the affected resonances by amounts < 20%. In order to detect these perturbations, difference spectra are calculated in which the normal spectrum is subtracted from a spectrum displaying the NOE effect. The sign and magnitude of the NOE are dependent on many factors; of prime importance to this discussion is the dependence on $r_{s,d}^{-6}$, where $r_{s,d}$ is the distance between the saturated, 's', and detected hydrogens, 'd', respectively. In general, hydrogens within approximately 3 A will show measurable enhancements; however, in some cases the effects can extend further.

As an example of how the NOE experiment reveals the relative spatial orientation of different hydrogens, NOE difference spectra for βDMan*p*1-OMe, on irradiation of different hydrogens, are shown in Fig 1. When H1 is irradiated NOE's are observed on the H2, H3, H4, H5 and OMe. H1 is within 2.6 A of H2, H3, H5 and the OMe so that large direct NOE's are expected; however, H4 is 3.9 A from H1 and therefore would not be expected to show an NOE. The small NOE on H4 arises because it is strongly coupled to H3 which experiences a large direct NOE. Because of the strong coupling the spin states of H3 and H4 are mixed and cannot be considered to be indepedent. Thus some of the NOE on H3 is distributed to H4.

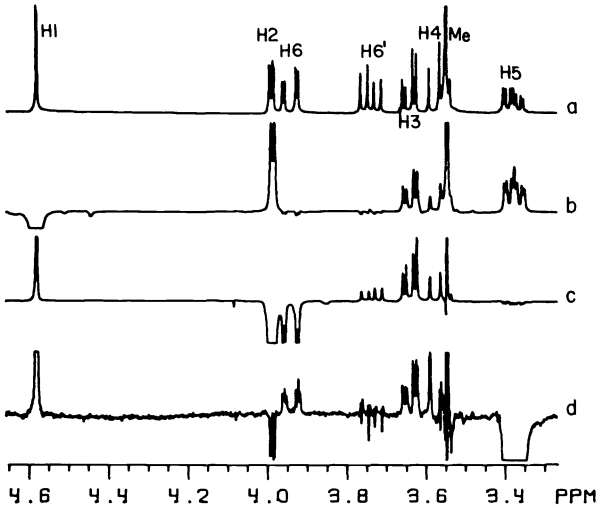

FIGURE 1: The results of one-dimensional equilibrium NOE measurements for βDMan*p*1-OMe: (a) Normal 360 MHz ^{1}H NMR spectrum; (b)-(d) Difference NOE spectra on irradiation of H1, H2 and H5, respectively.

An additional complicating factor in the interpretation of NOE's is the existence of 'three-spin effects'. Hydrogens which are dipolar coupled (close in space) to a hydrogen experiencing a large direct NOE will show an NOE, despite the fact that they are not close to the irradiated hydrogen. These NOE's are termed 'three-spin effects' and are always negative, whereas direct NOE's are positive for small, rapidly-tumbling molecules (trisaccharides or smaller at 360 MHz) and negative for large, slowly-tumbling molecules. An example of a three-spin effect is shown in Fig 1c where the NOE's on irradiation of the H5 can be seen. The negative NOE on H2 results from the three-spin effects generated by the direct NOE's to the H1 and H3. It must be emphasized that in any NOE experiment the resulting NOE on a particular resonance may arise as a summation of several three-spin contributions in addition to a direct effect. This is particularly true for β-pyranoses. Thus, interpretation of the magnitude of the NOE as if it were solely a direct NOE will give rise to severe errors in distance estimation (for a detailed discusson see ref. 7). However, starting with known geometry it is possible to calculate all the NOE'S <u>including three-spin effects</u> and thus by comparing observed NOE's to those calculated for different geometries it is possible to deduce those geometries consistent with the observed NOE's. The comparison between observed and calculated NOE's shown in Table 1 illustrates that the theory is capable of accurately reproducing the observed values when the geometry is known. Note that the negative three-spin effect on H2 is also correctly calculated. To illustrate the importance of taking three-spin effects into account, Table 2 lists a breakdown of the individual contributions to various NOE's of importance in the determination of the torsional angles for the Manα1,3 linkage of the biantennary complex class glycopeptide, GnGn(+F) (for an explanation of this nomenclature see ref. 16 and Fig. 2). Note, for example, that upon irradiation of the H1 of the Manα1,3, the direct NOE on the H2 of the Manβ1,4 is less than 20% of the total NOE observed. Neglect of the three spin terms in this case would lead to large errors in the deduced distance between Mβ-H2 and M3-H1.

TABLE 1: Equilibrium NOE Values[a] for βDManp1-OMe.

		H1	H2	H3	H4	H5	H6	H6'	HMe
Absolute NOE	Obs.	-1	0.15	0.08	0.02	0.15	-	-	0.05
H1 saturated	Calc.	-1	0.18	0.06	0.00	0.14	-	-	0.03
Relative NOE	Obs.	1	-	1.6	0.3	-0.6[b]	-	0.4[b]	-
H2 saturated	Calc.	1	-	1.5	0.1	-0.3	-	0.0	-
Relative NOE	Obs.	1	-0.2	0.6	0.3	-	0.3	0.06	-
H5 saturated	Calc.	1	-0.3	0.9	0.4	-	0.5	-0.09	-

[a]The average errors for the observed absolute NOE values are ± 20%. The NOE's were quantitated by setting the intensity of the saturated resonance for one proton in the NOE difference spectra at -1. For a relative NOE, the intensity of the reference NOE is set at 1. This Table is taken from ref. 2 which should be consulted for a discussion of the parameters involved in the calculations: (phi,psi) = (-50,40), τ_c = 0.5 x 10^{-10} s, τ_r = 1 x 10^{-13} s, R^s = 0.03 s^{-1}.
[b]The effects from partial saturation of H6' have been neglected.

TABLE 2: Direct and Three-Spin Contributions to observed NOE's for the Manα1-3 linkage of a complex oligosaccharide[a].

Irradiation of M3-H1										Total
	Mβ-H1	Mβ-H2	Mβ-H3	Mβ-H4	Mβ-H5	M3-H2	M3-H3	M3-H4	M3-H5	NOE
Mβ-H1	**-0.2**	-	-1.6	-	-0.1	-	-	-	-	-2.0
Mβ-H2	-	**-0.4**	-1.4	-	-	-	-	-	-0.2	-2.2
Mβ-H3	-	-	**-13.1**	-	-	-	-	-	-	-13.3

Irradiation of Mβ-H2										Total
	Mβ-H1	Mβ-H3	Mβ-H4	Mβ-H5	M3-H1	M3-H2	M3-H3	M3-H4	M3-H5	NOE
Mβ-H3	-0.9	**-8.6**	-	-0.1	-0.1	-	-	-	-0.4	-10.1
M3-H1	-0.2	-1.8	-	-	**-0.6**	-	-	-	-0.4	-3.1
M3-H2	-	-0.2	-	-	-0.1	**-0.1**	-0.1	-	-0.4	-1.0
M3-H3	-	-0.1	-	-	-	-	**-0.9**	-	-2.5	-3.6
M3-H5	-0.1	-0.2	-	-	-	-	-0.1	-	**-18.7**	-19.0

[a] The calculations are for GnGn(+F) using a fixed geometry with phi, psi = -50°, -20° for the Manα1,3 linkage. The matrix is arranged to show the separate contributions of direct (bold-face) and three-spin effects (off-diagonal) to the total NOE (last column), τ_c = 1.0 x 10^{-9} s.

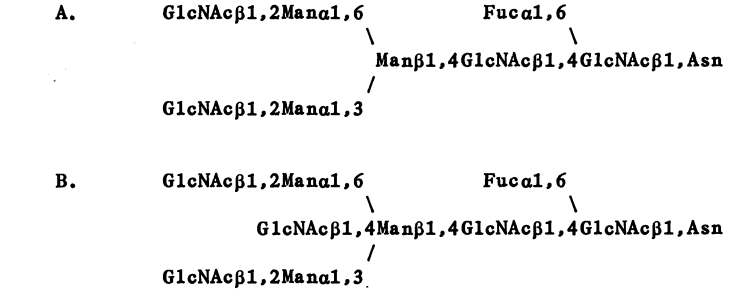

FIGURE 2: The structures of the biantennary complex class glycopeptides: (A) GnGn(+F); and, (B) bisected-GnGn(+F).

Deduction of geometry from quantitative NOE measurements

In our previous studies (refs. 2-7), we have used a method based on the superimposition of contour maps for the determination of the torsional angles consistent with all the observed NOE data. These contour maps were obtained by plotting the NOE's calculated for a particular experiment as a function of the torsional angles phi and psi (H1-C1-OX-CX and C1-OX-CX-HX, respectively where X refers to the number of the carbon at which the glycosylation occurs). We then outlined on the contour map the region of phi and psi values for which the calculated values corresponded to the range of values defined by the observed value plus or minus the experimental error. Generally each experimental result defined a slightly different area of 'allowed' phi/psi values. By superimposing all these areas of allowed values we could determine from the overlapping area the range of values defining the three-dimensional structures consistent with all the experimental results. These ranges differed somewhat depending on the size of the NOE's and the nature of the NOE contour plots but were usually on the order of $\pm 10^{\circ}$. Furthermore, these NOE-derived conformations were generally found to be centred on the minimum energy conformations estimated by various potential energy calculations. We interpreted these results as indicating, 'that motional averaging is confined to a narrow range about one stable conformation' (ref. 2). However, three years later, it is now apparent that this conclusion is not justified in all cases and that conformational flexibility must be incorporated into the theoretical treatment (refs. 8, 9).

Virtual conformations

In recent calculations we have encountered NOE-determined three-dimensional structures which differed significantly from any minimum energy conformation, using a variety of potential energy functions (refs. 8, 9). In these cases we were forced to conclude that the NOE-defined conformations corresponded to what Jardetzky (ref. 17) has termed 'virtual' conformations since they correspond to three-dimensional structures which few, if any, of the molecules in solution actually adopt. These conditions arise when the flexibility in the oligosaccharide is such that a wide range of conformations and hence NOE values are sampled during the course of the measurement. It became clear that for these molecules it was essential that this kind of conformational averaging be incorporated into the calculations. It also raised the question as to what extent averaging would influence the interpretation of the results for other molecules. Fortunately the theoretical basis of such effects had already been laid by Noggle and Schirmer (ref. 15).

Noggle and Schirmer have considered two cases of conformational averaging, in both of which the rate of internal motion is slow with respect to the molecular tumbling time. The two cases are distinguished according to whether the internal motion is fast or slow compared to the rate of NOE build up. For oligosaccharides and glycopeptides, the former is clearly the case. Under such circumstances the molecular geometry is varying during the course of the NOE measurement. If one assumes that all molecules sample all states during the course of the measurement, then the observed NOE can be predicted by calculating Boltzman-weighted averages over all states of the inverse sixth powers of the internuclear distances and then using these to solve for the NOE's. Thus the predicted NOE's become dependent on the potential energy functions used to obtain the Boltzman weighting factors and this dependence can be used to evaluate the appropriateness of the choice of functions in any particular situation.

For example, in Figs. 3A and 4A are shown the potential energy surfaces obtained for the Manα1,3 linkage of GnGn(+F). In the calculations from which Fig. 3A was generated, the HSEA functions (ref. 18) were used; whereas, in those for Fig. 4A, a hydrogen bond potential (ref. 19) was added (HEAH, refs. 8, 9). For the HSEA potential there is a minimum of -1.86 Kcal at (phi, psi) = $(-48^{\circ}, -18^{\circ})$ with a valley of low energy states extending from the minimum into regions of positive psi, while keeping phi essentially the same. When this energy surface is converted to a probability surface using the Boltzman distribution (ref. 9), the probability associated with the lowest energy state is found to be only 0.013. Thus, only about one percent of the time are the molecules found with the phi, psi values associated with the global minimum. In fact this potential predicts that the molecules sample a significant range of psi values ($\pm 20^{\circ}$ and $\pm 45^{\circ}$ for the 0.5 and 0.99 probability contours, respectively). The range is narrower for phi: $\pm 10^{\circ}$ and $\pm 25^{\circ}$, for probabilties of 0.5 and 0.99, respectively. When the hydrogen bond potential is included quite a different picture emerges (Fig. 4A). A new global minimum appears at phi, psi = -30°, 60° with a depth of -2.75 Kcal and an associated probability of 0.044. This minimum arises through the formation of two hydrogen bonds from the C2-OH of the Manβ1,4 to the O5 and C6-OH of the Manα1,3. Despite these two hydrogen bonds, the integrated probability associated with this new well is 0.25. Thus, according to this potential, the molecules spend 75% of the time in conformations which do not form these hydrogen bonds.

The three-dimensional structures corresponding to the minimum energy lattice points within the two different wells are shown in Figs. 3B (HSEA) and 4B (HEAH). In view of the considerable differences in the geometry associated with these two conformations, one might expect that the ensemble averaged NOE's derived from the two surfaces would be quite different. Thus, from a comparison with the observed values, it might be possible to determine which potentials give the best representation of the actual situation.

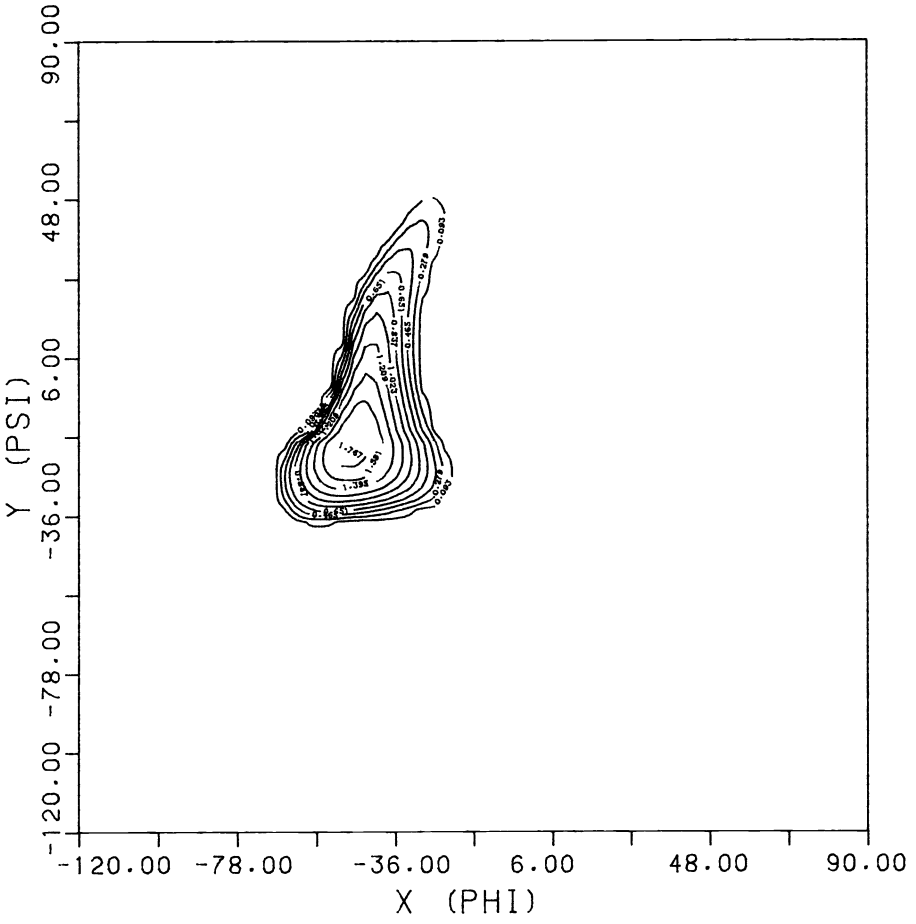

FIGURE 3A: The HSEA Potential Energy Surface for the Manα1,3 linkage of GnGn(+F).

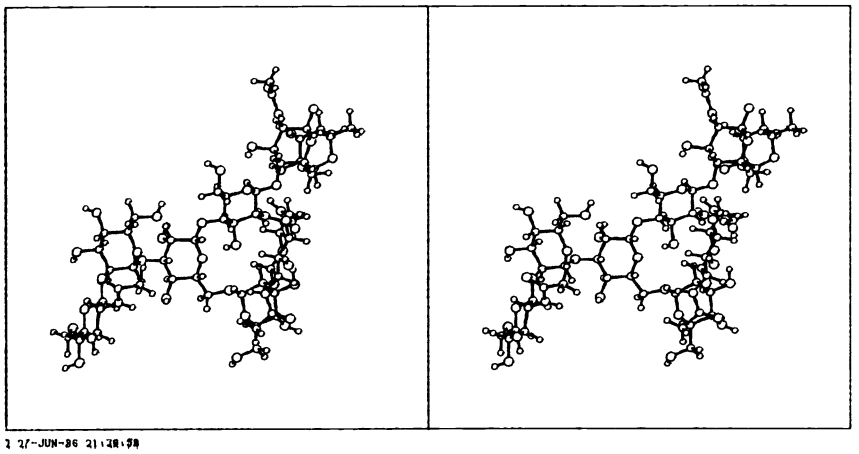

FIGURE 3B: The Three-Dimensional Structure Corresponding to the Minimum energy in the HSEA potential energy well: phi, psi = -48°, -18°. The fucosylated chitobiose core is on the upper right, the Manα1,3-arm is on the left and the Manα1,6-arm is on the lower right. The ω value for the latter has been set to -60°. Note the proximity of Mβ-H2 and M3-H5.

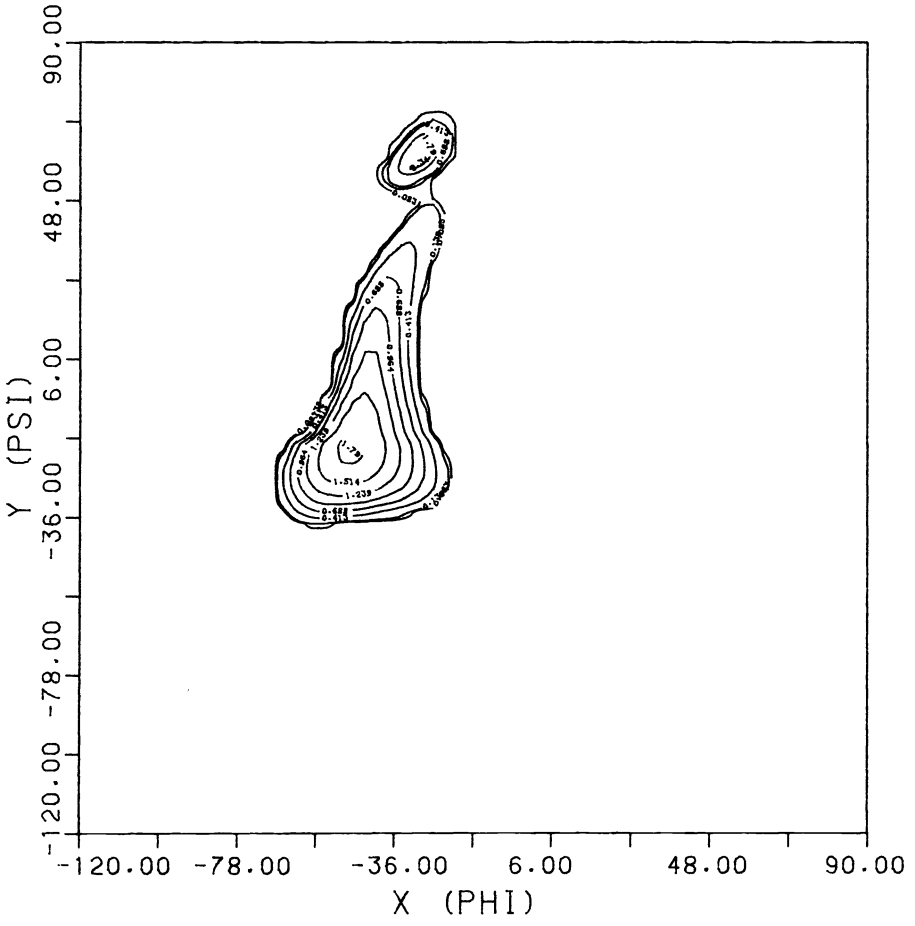

FIGURE 4A: The HEAH Potential Energy Surface for the Manα1,3 linkage of GnGn(+F).

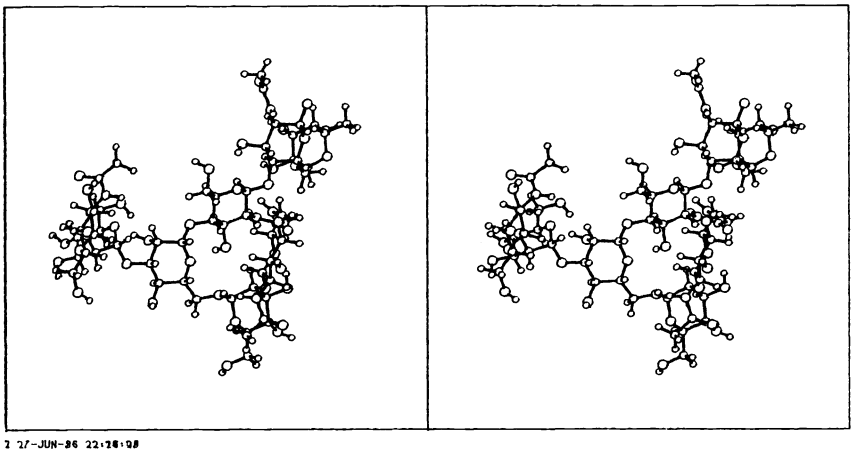

FIGURE 4B: The Three-Dimensional Structure Corresponding to the Minimum energy in the HEAH potential energy well: phi, psi = -30°, 60°. The fucosylated chitobiose core is on the upper right, the Manα1,3-arm is on the left and the Manα1,6-arm is on the lower right. The ω value for the latter has been set to -60°.

Because there are 54 non-exchangeable hydrogens which must be considered, it is neccessary to calculate the 54x54 relaxation matrix for each of the 4900 lattice points used to obtain the potential energy surface. The Boltzman weighted average relaxation matrix is then calculated and used to solve for the ensemble averaged NOE's (Table 3). The values obtained with a fixed geometry corresponding to the minimum energy lattice point in the HSEA well are also given for comparison. In this case, the latter NOE's differ little from the ensemble averaged values obtained with the HSEA potential. However, this is not true for all linkages since the degree of agreement will depend on how steeply the NOE values vary with (phi, psi). Comparison of the ensemble averaged NOE's obtained with the two different potential energy functions, shows that there is at least one NOE which differs significantly between the two sets of results (shown in boldface in Table 3). Taking the ratio of the NOE on Mβ-H2 to that on Gn-H1 (upon irradiation of M3-H1) one obtains 0.20 and 0.52 for the HSEA and HEAH potentials, respectively. Similarly, on irradiation of Mβ-H2 the ratios of the NOE's on M3-H1 and Mβ-H1 are 0.33 and 0.83 for the HSEA and HEAH potentials, respectively. Preliminary experimental values for these ratios for GnGn(+F) are 0.25±0.07 (irradiation of M3-H1) and 0.42±0.12 (irradiation of Mβ-H2). Both values are clearly in better agreement with the results generated from the HSEA potential, suggesting that in this case the hydrogen bonded conformations are occupied to a negligible extent. For other structures we have found the opposite result. At the moment, therefore, it is necessary to consider each compound separately.

TABLE 3: Ensemble averaged NOE's[a] for the Manα1,3 linkage of GnGn(+F) using the HSEA and HEAH potentials.

	Mβ-H1	Mβ-H2	Mβ-H3	Mβ-H4	Mβ-H5	M3-H2	M3-H3	M3-H4	M3-H5	Gn-H1
Irradiation of M3-H1										
Fixed[b]	-2.0	-2.2	-13.3							
HSEA	-1.2	**-2.8**	-14.3	-2.7	-1.3	-12.3	-3.9	-1.7	-2.1	-14.2
HEAH	-1.6	**-7.3**	-14.5	-2.5	-1.3	-12.3	-4.0	-1.7	-2.6	-14.1

	Mβ-H1	Mβ-H3	Mβ-H4	Mβ-H5	M3-H1	M3-H2	M3-H3	M3-H4	M3-H5
Irradiation of Mβ-H2									
Fixed[b]		-10.1			-3.1	-1.0	-3.6		-19.0
HSEA	-7.2	-8.7	-2.5	-1.5	**-2.4**	-1.0	-2.8	-1.3	-13.5
HEAH	-7.2	-9.3	-2.6	-1.6	**-6.0**	-1.5	-2.5	-1.3	-11.3

[a] $\tau_c = 1.0 \times 10^{-9}$ s. The NOE's which differ for the two potentials are shown in boldface. [b] Calculations as for Table 2.

Orientation of the Manα1, 6-arm

The relatively restricted flexibility of the Manα1,3-arm of the N-linked oligosaccharides contrasts with the more extreme reorientations found to be possible for the Manα1,6-arm. The extra torsional angle for 1,6 angles was the reason cited by Montreuil (ref. 1) in his original hypothesis and indeed it is this angle, ω (O6-C6-C5-H5), that can take on two very different values in GnGn(+F). In most 1,6 linkages psi also is relatively unrestricted (refs 8, 20). However, as the oligosaccharides become more branched and/or more compact, the opportunities for additional interactions increase. Such long range interactions have been found to considerably restrict the 1,6 linkage in $Man_6GlcNAc_2Asn$ (ref. 3) and in $Man_9GlcNAc_2Asn$ (ref. 9), for example. Hence every case must be considered separately. The overall situation for the Manα1,6 linkage of GnGn(+F) can be represented as a three-dimensional iso-energy surface in conformational space. Figure 5 shows in stereo the surface obtained using the HSEA (ref. 18) potential energy functions modified (ref. 9) to include the Hassel-Ottar effect (ref. 21). The ω axis runs upward to the right starting at 120° and decreasing to -240°. Thus the regions corresponding to the three possible staggered rotamers about the C5-C6 bond (see ref. 3) occupy the first, second and third thirds of the cube (ω = +60°, -60° and 180°, respectively). The low energy conformers are confined to the regions corresponding to ω = 180° and -60°. There is a connection between the two lobes of the surface indicating that interconversion would be expected and the analysis of the $J_{5',6}$ coupling constant by many laboratories (refs 3, 10-12) supports this conclusion. Conversion of the potential energy values to probabilities with subsequent summation over the two lobes, yields relative populations for the two allowed rotamers of 6:1 in favour of the ω = 180° form. This result is at odds with the observed ratio of approximately 1:1, suggesting that there are problems with the potential energy functions used. This issue will be discussed in detail elsewhere (ref. 9). In Fig. 6 a stereo representation of the postulated three-dimensional structures corresponding to the two C5-C6 rotamers is given. The position of the Manα1,6-arm in the two conformers is clearly quite different.

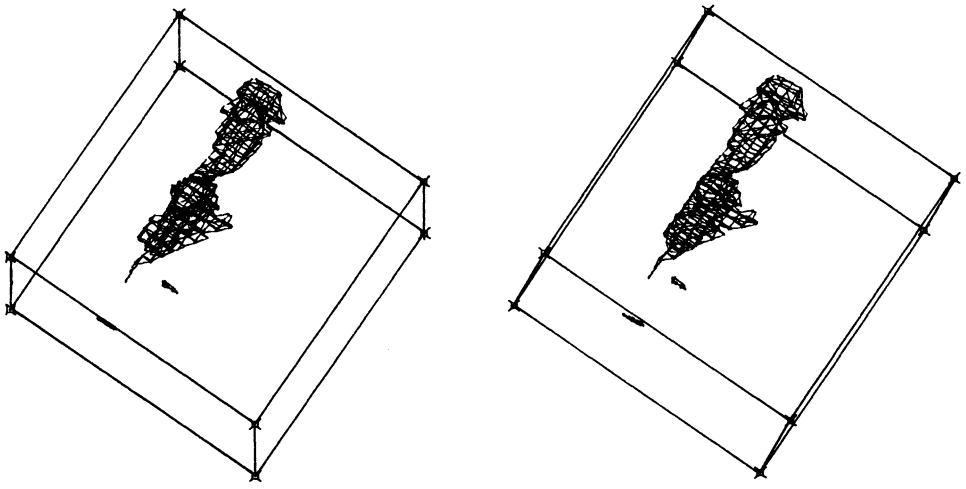

FIGURE 5: A stereo representation of the iso-energy surface for the Manα1,6 linkage of GnGn(+F). The surface shown is for an energy 7 Kcal above the global minimum and the probability of a molecule having a conformation located within this surface is greater than 0.99.

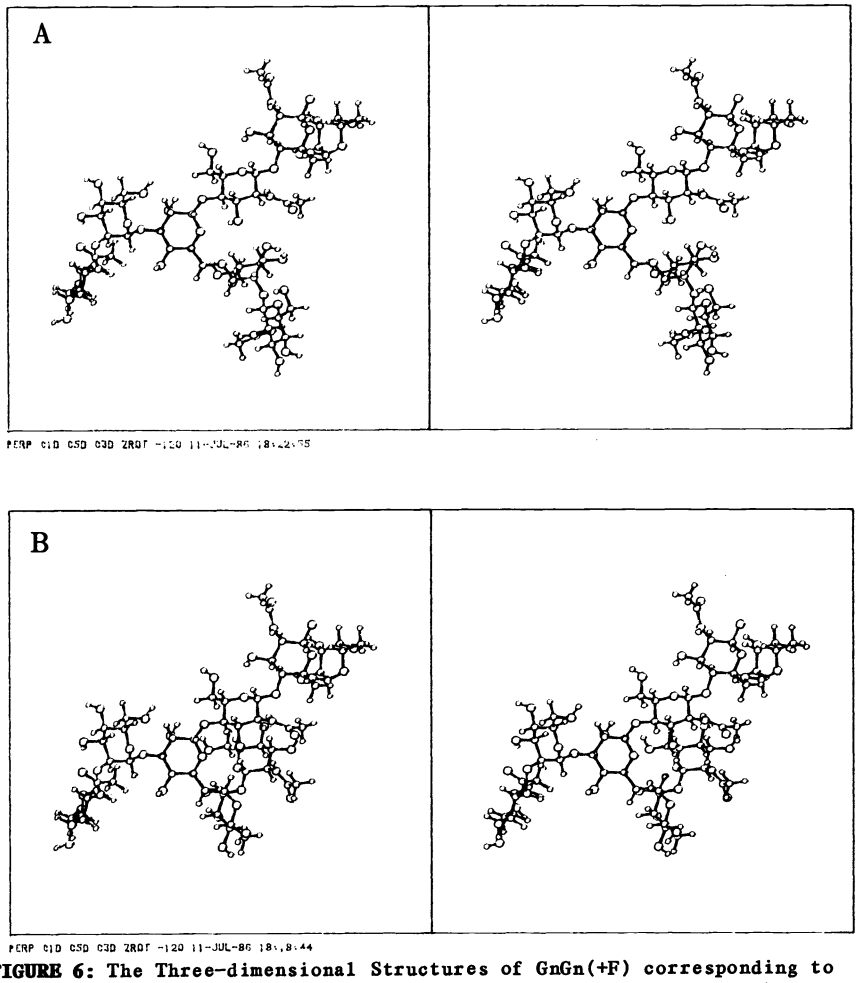

FIGURE 6: The Three-dimensional Structures of GnGn(+F) corresponding to the two different values of ω: (A) ω = -60°; (B) ω = 180°; (phi, psi) values are from ref. 5.

The above results are in striking contrast to those found for the bisected counterpart of GnGn(+F). Here the $J_{5,6}$ coupling constant was found to be consistent with primarily one C5–C6 rotamer being present, that with ω = 180° (ref. 3). The corresponding three-dimensional structure is shown in Fig. 7. The Manα1,6-arm is folded back over the core of the glycopeptide. In Fig. 8, the potential energy cube (using the HSEA functions) for bisected-GnGn(+F) is shown. As with GnGn(+F), there are essentially two allowed regions corresponding to the same two C5–C6 rotamers. However, in this case there is no low energy connection between them, in fact the barrier is 16 Kcal at its lowest point. Taking together the experimental observation of only one rotamer and the lack of a connection between the two low energy regions in the potential energy cube, we have made some specific predictions (ref. 5) about the specificity of GlcNAc-tranferase III (Gn-T III, ref. 22), the enzyme which converts GnGn(+F) to bisected-GnGn(+F).

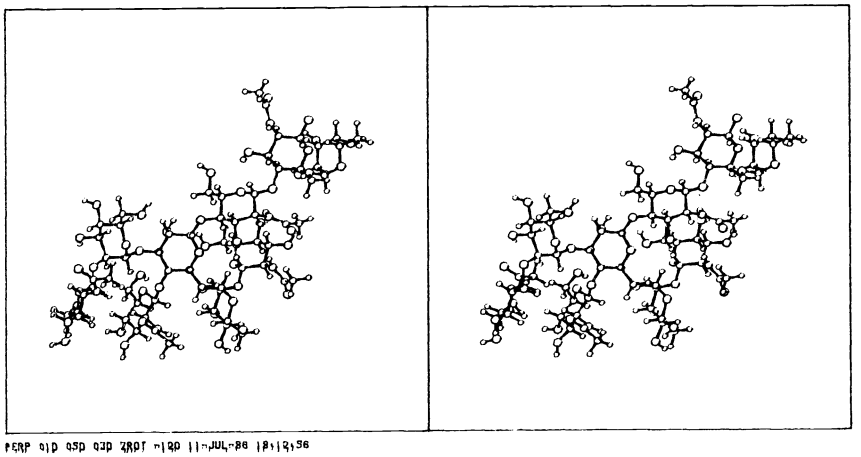

FIGURE 7: A stereo representation of the three-dimensional structure of the lowest energy form of bisected-GnGn(+F) with ω = 180°. The (phi, psi) values are from ref. 5.

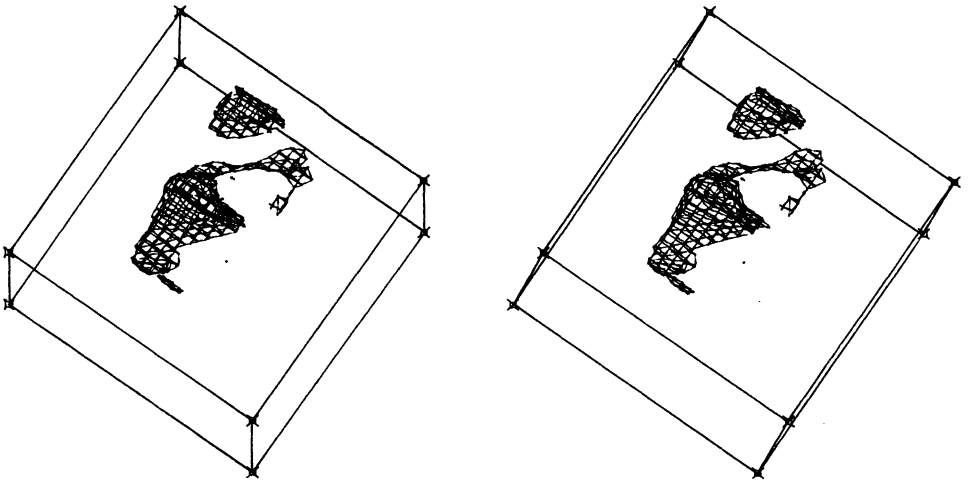

FIGURE 8: A stereo representation of the iso-energy surfaces for the Manα1,6 linkage of bisected-GnGn(+F). The surfaces shown correspond to values 9 Kcal above the global minimum and the calculated probability of a linkage conformation being within these surfaces is greater than 0.99.

SITE-DIRECTED PROCESSING

Substrate specificity of GlcNAc-transferase III

The substrate specificity of an enzyme is usually thought of in terms of the primary structure characteristics of the substrate required for maximal enzyme activity. In situations where the substrates exist in more than one three-dimensional form, an additional issue is, 'Which of the three-dimensional structures is the best substrate?'. This distinction became of interest when we found (ref. 3) that the biantennary complex class of

N-linked oligosaccharides existed in two major three-dimensional forms whereas the bisected biantennary complex class appeared to be confined to only one such class - that in which the Manα1,6-arm of the molecule was folded back over the chitobiose core (Figure 7).

This result suggested that Gn-T III might have a preference for the three-dimensional form of the biantennary substrate with the 6-arm folded back and, because of the 16 Kcal barrier, the product would not interconvert to the $\omega = -60°$ form. Thus, only the $\omega = 180°$ conformer would be found, despite the fact that low energy conformers exist for both rotamers. This interpretation suggested a mechanism for the control of processing at individual glycosylation sites on glycoproteins (ref. 23).

Site-directed processing

It has been known for some time that, for glycoproteins with more than one glycosylation site, the oligosaccharide structures at the different sites are often very different (ref. 24). Since the oligosaccharide structures attached to a given polypeptide will be exposed to the same set of processing enzymes, the existence of different structures at these sites must result from the influence of the differences in the protein three-dimensional structure around the different glycosylation sites. What has not been clear was the mechanism whereby the protein structure influences processing. There have been several attempts at explaining this phenomenon but none can account for all the known facts. Pollack and Atkinson (ref. 24) observed that there is a gradient in the degree of processing such that the sites closer to the N-terminal of the glycoprotein were more processed than those towards the C-terminal. They suggested that, since the protein is synthesized from the N-terminal end, the protein would be less complete and possibly less folded at the time of glycosylation and therefore the oligosaccharide might be more accessible to the processing enzymes; alternatively, proximity to the membrane might inhibit C-terminal processing. These may well be general mechanisms, but there clearly are exceptions which suggest that further effects come into play in specific instances. Another model has been proposed which also suggests that differential accessibility is at the root of differential processing (refs. 25, 26). This model arose from the observation that the extent processing was correlated with the extent of sensitivity of an oligosaccharide to digestion by endoglycosidase H, an enzyme that cleaves the structures close to the point of attachment to the Asn side chain. Because of the sequential nature of the oligosaccharide biosynthetic pathway, these accessibility models would predict that the structures present at the different sites of a given glycoprotein would represent different stages along a single processing pathway. However, as the pathway has a number of branches (for a review see ref. 27) a different mechanism is required to explain why different sites on a glycoprotein would have structures representing the products located on different branches of the processing pathway.

We found a particular human myeloma IgG(Hom) which provided an example of two sites with oligosaccharide structures which are the result of different pathways (ref. 23). At Asn 107 of the light chain the oligosaccharides are all of the Neu5Acα2,6-terminated, bisected-biantennary complex class whereas those at the Asn 297 of the heavy chain are primarily of the biantennary complex class without a bisecting GlcNAc and terminating in Gal or Neu5Ac. It is known from the substrate specificity studies of Narasimhan (ref. 22) that Gn-T III must act before galactosylation occurs. Thus, if inaccessibility due to protein folding were the cause for the absence of bisected structures at Asn 297 then the oligosaccharide should also be inaccessible to the galactosyl and sialyl transferases that are known to act later in the pathway. Yet the majority of structures at Asn 297 are galactosylated and sialylated. The resolution of this apparent anomaly lies in the recognition that interactions with the protein surface could stabilize the oligosacharide at Asn 297 in the $\omega = -60°$ form such that it is not in the right three-dimensional conformation to be a substrate for GlcNAc transferase III. This hypothesis is confirmed by the X-ray diffraction study of the human myeloma F_c fragment (ref. 28) which shows the oligosaccharide in the $\omega = -60°$ form.

This explanation for the differential processsing of the two glycosylation sites of human IgG(Hom) suggested that this same mechanism might be more general and, if so, that it would provide a means whereby additional specificity could be conferred on the processing at individual sites. We decided therefore to call it 'Site-Directed Processing' in order to emphasize the role that the protein plays in determining the pathway of processing. The requirements for this mechanism to be operative at any particular step in processing are threefold:

(i) That more than one distinct three-dimensional structure be available to the oligosaccharide substrate;
(ii) That there be a processing enzyme for which only some of the available three-dimensional structures of the oligosaccharide are substrates; and,
(iii) That interaction with the protein environment at the glycosylation site preferentially stabilizes three-dimensional structures of the oligosaccharide which are not substrates for the enzyme.

When these three conditions are met then, despite the presence of that enzyme activity in the cell, that oligosaccharide will not be modified by that enyme and will be available as a substrate for other enzymes which might not otherwise have acted at that site. How many steps in the processing pathway might meet these conditions? It turns out that even from our limited knowledge of the three-dimensional structures of the intermediates in the glycosylation pathway, it is clear that there are a many opportunities for this mechanism to act. A summary of the possible steps is given in Table 4. Of course we do not know at this point the extent to which conditions (ii) and (iii) are satisfied for any of these additional possibilities. However, that information should rapidly become available as the library of crystal structures for glycoproteins grows larger. However, even at this stage it is possible to speculate as to which are the most likely steps at which the mechanism operates simply on the basis of the oligosaccharide structures commonly found among glycoproteins. For example, among the high mannose class of oligosaccharide structures, the most commonly occuring are the Man_{8-9} and Man_{5-6} size classes. Thus it would appear that steps 2, 4 and 5 are likely candidates.

TABLE 4: 'Site-directed' Processing Possibilities

Step	Enzymes[a]	Reaction catalyzed	Residue Reorienting[b]
1.	Man-T:	Man_8 --- Man_9(yeast)	Man_8 6i[c]
2.	Man'ase I:	Man_8 --- Man_7	Man_8 6i[c] or 6t[d]
3.	Man'ase I:	Man_7 --- Man_6	Man_7 6i[c] or 6t[d]
4.	Man'ase I:	Man_6 --- Man_5	Man_6 6i[c] or 6t
5.	Gn-T I:	Man_5 --- $Man_5Gn(I)$	Man_5 6i[c] or 6t
6.	Man'ase II:	$Gn(I)Man_5$ --- $Gn(I)Man_4$	$Gn(I)Man_5$ 6i[c] or 6t[d]
7.	Man'ase II:	$Gn(I)Man_4$ --- $Gn(I)Man_3$	$Gn(I)Man_4$ 6i[c] or 6t[d]
8.	Gn-T II:	MGn --- GnGn	MGn 6i
9.	Gn-T III:	GnGn --- bis-GnGn	GnGn 6i
10.	Gn-T IV:	GnGn --- tri-antennary	GnGn 6i
11.	Gn-T V:	GnGn --- tri'-antennary	GnGn 6i
12.	Gal-T, etc	bi-antennary --- +Gal or tri-antennary	6i

[a] See ref. 27 for a review of the enzyme nomenclature and specificities.
[b] 6i refers to the Manα1,6 residue linked to the Manβ1,4 of the core. 6t refers to the Manα1,6 residue linked to 6i residue.
[c] In isolated glycopeptides, after removal of the terminal Manα1,2 on the Manα1,3 of the Manα1,6-arm, the 6t is predicted to remain in the ω = 180° form while the 6i reorients from ω = 180° to ω = -60° . However, at
[d] any given glycosylation site this reorientation may not be favourable. Different isomers would be expected to behave differently.

Since all the mannosidase-I processing occurs before the Gn-T I branch point, site-specificity in this part of the pathway could be explained entirely by the reduced-accessibility models (refs. 25, 26). However, there are specific opportunities for the site-directed processing mechanism to be operative since many of the intermediates along this part of the pathway have been found to exist in more than one conformation (Table 4). In some cases there are relatively minor differences between the possible conformations such as the orientation of a terminal Manα1,6 residue (steps 3-6, ref. 3). In other cases the differences may be major, as in the reorientation that can occur between Man_9 and Man_8 which involves the entire Manα1,6 arm (steps 1 and 2, refs. 5, 9). Oligosaccharide modifications such as phosphorylation or sulfation would also be expected to be dependent on the three-dimensional structure of the oligosaccharide. Thus the site-directed processing mechanism would predict situations in which at some glycosylation sites phosphorylation occurs and at others it does not, despite the apparent presence of all the right signals. In addition, if the different mannosidase I enzymes in ER and Golgi (refs. 29, 30) have different specificities and/or three-dimensional requirements for optimal substrates, then the site-directed processing mechanism could control whether processing occurs in the ER or the Golgi. Clearly this could be important for the control of intracellular trafficking.

Further down the pathway, the branches to tri-, tri'- and tetra-antennary complex structures could be controlled by the particular three-dimensional structure of the substrates stabilized at a given glycosylation site. Here it is difficult to be more specific since the detailed substrate specificities of these enzymes has not yet been elucidated.

CONCLUSION

In summary, the three-dimensional structures of the N-linked oligosaccharides, show varying degrees of flexibility in different parts of the molecule. For many glycosidic linkages there are several minima in the potential energy surfaces obtained with different algorithms and it is necessary to determine experimentally whether the biologically synthesized molecule is distributed among all these low energy conformations or localized to a particular subset. In some of the latter situations the subset of low energy conformations consistent with experiment does not include the global minimum, suggesting that inappropriate potential functions have been used. In other cases alternate low energy conformations exist but are not accessible from the biologically synthesized three-dimensional structure. For these reasons the results of potential energy calculations with the N-linked oligosaccharides must be interpreted with extreme caution.

In agreement with Montreuil's prediction of a decade ago (ref. 1), the 1,6 linkages of the N-linked oligosaccharides are a major source of intramolecular flexibilty of biological significance. In particular, interactions with the protein at the glycosylation site may stabilize a unique subset of the three-dimensional structures otherwise accessible to the oligosaccharide. Since the processing enzymes require specific substrate three-dimensional structures for optimal activity, this phenomenon provides a possible explanation for the differential processing at the several glycosylation sites of a glycoprotein.

Acknowledgements

We thank Karl Hardman for his suggestion which initiated the development of this model and also the members of the Carver and Schachter laboratories for their comments. This work was supported by Grants from the Medical Research Council of Canada (MT-3732 and MT-6499) and the National Cancer Institute of Canada (Terry Fox Special Initiatives Program).

REFERENCES

1. J. Montreuil, B. Fournet, G. Spik and G. Strecker, C. R. Acad. Sci. Paris,287 Serie D, 873-840 (1978).
2. J.-R. Brisson and J.P. Carver, Biochemistry 22, 1362-1368 (1983).
3. J.-R. Brisson and J.P. Carver, Biochemistry 22, 3680-3686 (1983).
4. J.-R. Brisson and J.P. Carver, Biochemistry 22, 3671-3680 (1983).
5. J.-R. Brisson and J.P. Carver, Can. J. Biochem. 61, 1067-1078 (1983).
6. J.P. Carver and J.-R. Brisson, in: Biology of Carbohydrates, (V. Ginsburg and P.W. Robbins, eds.), John Wiley and Sons, New York, pp. 289-331 (1984).
7. J.P. Carver, D.A. Cumming and A.A. Grey, in Glycoprotein Structure and Conformation. (R.J. Ivatt, ed.), in press, (1986).
8. D.A. Cumming, R.N. Shah, J.J. Krepinsky, A.A. Grey and J.P. Carver, submitted.
9. D.A. Cumming and J.P. Carver, submitted.
10. K. Bock, J. Arnarp and J. Lonngren, Eur. J. Biochem. 129, 171-178 (1982).
11. H. Paulsen, T. Peters, V. Sinnwell, R. Lebuhn and B. Meyer, Liebigs Ann. Chem., 951-976 (1984).
12. H. Paulsen, T. Peters, V. Sinnwell, R. Lebuhn and B. Meyer, Liebigs Ann. Chem., 489-509 (1985).
13. R.U. Lemieux and K. Bock, Arch. Biochem. Biophys. 221, 125-134 (1983).
14. G.M. Lipkind, A.S. Shashkov and N.K. Kochetkov,Carbohydr. Res., 141, 191-19? (1985).
15. J.H. Noggle and R.E. Schirmer, The Nuclear Overhauser Effect, Academic Press, New York (1971).
16. J.P. Carver and A.A. Grey, Biochemistry 20, 6607-6616 (1981).
17. O. Jardetzky, Biochim. Biophys. Acta. 621, 227-232 (1980).
18. H. Thogersen, R.U. Lemieux, K. Bock and B. Meyer, Can. J. Chem. 60, 44-57 (1982).
19. S. Perez, personal communication.
20. I. Tvaroska, S. Perez and R.H. Marchessault, Carbohydr. Res., 61, 97-106 (1978).
21. R.H. Marchessault and S. Perez, Biopolymers, 18, 2369-2374 (1979).
22. S. Narasimhan, J. Biol. Chem. 257, 10235-10242 (1982).
23. G. Savvidou, M. Klein, A.A. Grey, K. Dorrington and J.P. Carver, Biochemistry. 23, 3736-3740 (1984).
24. L. Pollack and P.H. Atkinson, J. Cell Biol. 97, 293-300 (1983).
25. P. Hsieh, M.R. Rosner and P.W. Robbins, J. Biol. Chem. 258, 2555-2561 (1983).
26. R.B. Trimble, F. Maley and F.K. Chu, J. Biol. Chem. 258, 2562-2567 (1983).
27. H. Schachter, S. Narasimhan, P. Gleeson and G. Vella, G., Can. J. Biochem. and Cell Biol., 61, 1049-1066 (1983).
28. J. Deisenhofer, Biochemistry 20, 2361-2370 (1981).
29. I. Tabas and S. Kornfeld, J. Biol. Chem. 254, 11655-11663 (1979).
30. J. Bischoff and R. Kornfeld, J. Biol. Chem. 258, 7907-7910 (1983).